INTERNATIONAL JOURNAL FOR NUMERICAL METHODS IN FLUIDS, VOL. 4, 1165–1184 (1984)

BUOYANCY EFFECTS ON TURBULENT SWIRLING FLOWS

H. S. TAKHAR AND M. A. HALIM*

University of Manchester, Simon Engineering Labs, Oxford Road, Manchester M13 9PL, U.K.

SUMMARY

A three-parameter model of turbulence applicable to free boundary layers has been developed and applied for the prediction of axisymmetric turbulent swirling flows in uniform and stagnant surroundings under the action of buoyancy forces. The turbulent momentum and heat fluxes appearing in the time-averaged equations for the mean motion have been determined from algebraic expressions, derived by neglecting the convection and diffusion terms in the differential transport equations for these quantities, which relate the turbulent fluxes to the kinetic energy of turbulence, k, the dissipation length scale of turbulence, L, and the temperature covariance, $\bar{T}'^2$. Differential transport equations have been used to determine these latter quantities. The governing equations have been solved using fully implicit finite difference schemes. The turbulence model is capable of reproducing the gross features of pure jet flows, buoyant flows and swirling flows for weak and moderate swirl.

The behaviour of a turbulent buoyant swirling jet has been found to depend solely on exit swirl and Froude numbers. The predicted results indicate that the incorporation of buoyancy can cause significant changes in the behaviour of a swirling jet, particularly when the buoyancy strength is high. The jet exhibits similarity behaviour in the initial region for weak swirl and weak buoyancy strengths only, and the asymptotic case of a swirling jet under the action of buoyancy forces is a pure plume in the far field. The predicted results have been found to be in satisfactory agreement with the available experimental data and in good qualitative agreement with other predicted results.

KEY WORDS Turbulence Buoyancy Swirl

INTRODUCTION

A buoyant swirling jet, emitted into an otherwise stagnant surrounding may be produced by discharging a fluid, whose density is different from that of the environment, with azimuthal as well as axial velocity from a vertical nozzle or an orifice. The degree of swirl imparted to the jet may be characterized by the ratio of the azimuthal to the axial velocity at the jet exit, and the buoyancy strength of the jet is determined by the magnitudes of the axial velocity and the density (or temperature) difference between the jet centre and the environment at the source. The large-scale effects of swirl on the rate of spread, mixing and penetration of a non-buoyant jet suggest that the practically important cases of buoyant flows (e.g. the flow patterns associated with the environmental pollution) could be managed more efficiently with the aid of swirl.

In the past the prediction of the characteristics of free jet flows, with or without the effect of swirl and or buoyancy, was most commonly done by employing integral methods. Recently, however, emphasis has shifted towards the use of differential methods. Both of these methods are based on

*Present address: Department of Water Resources Engineering, Bangladesh University of Engineering & Technology, Dhaka-2, Bangladesh

0271–2091/84/12 1165–20$02.00

Received 1 March 1983
Revised 14 February 1984

the laws of conservation of mass, momentum and energy or species concentration which are expressed in terms of partial differential equations. The integral methods assume empirical profile shapes for velocity, temperature or concentration, so that the partial differential equations can be integrated over the jet cross-section to yield ordinary differential equations describing the axial variation of some characteristic velocity and density. The system of equations is normally closed by making an assumption about the entrainment of ambient fluid into the turbulent jet. The integral methods are difficult to extend to more complex turbulent flows in which it is often difficult to prescribe the profile shapes and to relate the entrainment rate to the local parameters that influence this rate.

The prediction of the flow characteristics of turbulent swirling plumes, in an otherwise still environment, using integral methods was undertaken by Lee,[1] Narain and Uberoi[2] and Ross.[3] Lee and Ross postulated a direct relationship between the unknown entrainment and the mean flow variables based on physical and dimensional arguments, whereas Narain and Uberoi achieved the closure indirectly by considering an additional equation for the conservation of mechanical kinetic energy.

The differential methods, on the other hand, do not employ profile and entrainment assumptions but obtain the profile and entrainment rates as part of the solution. In general, these methods are constituted by the same partial differential equations as those used in the integral methods but the closure of the governing equations is achieved by introducing assumptions about the turbulent processes in order to determine the extra terms representing the turbulent fluxes of momentum and heat or species concentration appearing in the governing partial differential equations. These assumptions form a turbulent model which, in contrast to the global profile and entrainment assumptions in integral methods, describes the state of turbulence at each point in the flow and is therefore essentially much more general. Normally, the performance of a differential method depends entirely on the turbulence model it employs.

Turbulence models of various levels of complexity have been reported in the literature. The simplest ones, such as the well-known Prandtl mixing-length hypothesis, relate the turbulent fluxes directly to the local mean flow quantities whereas the most complex models solve differential transport equations for the individual fluxes. However, only a few of these turbulence models have been used for predicting the flow characteristics of turbulent jets with or without the effects of swirl or buoyancy. Rodi and Spalding[4] developed a two-parameter (k–kL) model for predicting free jet flows. Lilley[5] developed two anisotropic eddy viscosity models for predicting turbulent swirling flows—one an extended Prandtl mixing-length model and the other a two-parameter (k–kL) model. Chen and Rodi[6] modified Launder's[7] model proposals and Madni and Pletcher[8] used a mixing-length model for predicting vertical buoyant jets in uniform and stratified environments. Launder and Morse[9] presented an in-depth study of swirl problems with a high-order Reynolds stress closure model. Chen and Nikitopoulos[10] used Chen and Rodi's[6] model for predicting the near-field region characteristics of a vertical buoyant jet in a uniform environment.

The aim of the present work is to develop and test a three-parameter (k–kL–$\overline{T'^2}$) model of turbulence for predicting the flow characteristics of a turbulent swirling jet in uniform and stagnant surroundings under the action of buoyancy forces. This work may be considered as an extension of Lilley's[5] work for the prediction of non-buoyant swirling flows using a two-parameter (k–kL) model of turbulence.

DEVELOPMENT OF THE TURBULENCE MODEL

We consider a steady low Mach number jet produced by discharging a fluid with azimuthal as well as axial velocities and having its axis aligned with the gravity vector. The density of the jet is

different from that of the environment so that it is subject to buoyancy forces. Furthermore, it will be assumed that the jet is remote from the walls, is generated from a single finite source and is issuing into a stagnant surrounding.

In a cylindrical polar co-ordinate system (r, θ, z), with the z-axis pointing vertically upwards and with associated mean velocities, u, v and w, in these directions, the governing equations for steady $(\partial/\partial t = 0)$ and axisymmetric $(\partial/\partial\theta = 0)$ turbulent mean motion, employing the usual boundary layer approximations $(\partial/\partial r \gg \partial/\partial z)$, reduce to:[11]

Continuity

$$\frac{1}{r}\frac{\partial ru}{\partial r} + \frac{\partial w}{\partial z} = 0 \tag{1}$$

Radial momentum

$$\frac{v^2}{r} = \frac{1}{\rho}\frac{\partial p}{\partial r} \tag{2}$$

Swirl momentum

$$u\frac{\partial v}{\partial r} + w\frac{\partial v}{\partial z} + \frac{uv}{r} = -2\frac{\overline{u'v'}}{r} - \frac{\partial}{\partial r}(\overline{u'v'}) \tag{3}$$

Axial momentum

$$u\frac{\partial w}{\partial r} + w\frac{\partial w}{\partial z} = -\frac{1}{\rho}\frac{\partial p}{\partial z} + \frac{g}{\rho}(\rho_a - \rho) - \frac{\overline{u'w'}}{r} - \frac{\partial}{\partial r}(\overline{u'w'}) \tag{4}$$

Energy

$$u\frac{\partial T}{\partial r} + w\frac{\partial T}{\partial z} = -\frac{\overline{u'T'}}{r} - \frac{\partial}{\partial r}(\overline{u'T'}) \tag{5}$$

In the above equations, p, T and ρ are the time-averaged pressure, temperature and density respectively, g is the acceleration due to gravity, the subscript 'a' denotes the ambient condition, an overbar indicates a time-averaged quantity and a prime denotes the deviation from that average. In deriving equations (1) to (5), the usual Boussinesq approximation, in which the density variation is accounted for only in the gravitational term, has been employed and it has been assumed that in free turbulent flows the laminar terms are much smaller in magnitude than the corresponding turbulent quantities.

An inspection of the equations (1) to (5) reveals that they contain a number of unknown functions of turbulence correlations. Therefore, before these equations may be used for predictive purposes, it is necessary that the unknown turbulence correlations must be rewritten in terms of calculable quantities.

First consider the Reynolds stress component $\overline{u'w'}$. The differential transport equation for this correlation has been given by Launder.[7] In the present investigation this equation is simplified by neglecting the convective and diffusive transport terms of $\overline{u'w'}$ to give

$$0 = \overline{u'^2}\frac{\partial w}{\partial r} - \frac{g}{T_a}\overline{u'T'} + \frac{\varepsilon}{C'k}\overline{u'w'} \tag{6}$$

where C' is a constant and ε is the rate of dissipation of the turbulence kinetic energy by viscous action. For high Reynolds number turbulence, the dissipation rate ε is given by

$$\varepsilon = C_\varepsilon \frac{k^{3/2}}{L} \tag{7}$$

where C_ε is a constant. Using equation (7), equation (6) may be recast as

$$-\overline{u'w'} = \frac{\mu_{rz}}{\rho}\frac{\partial w}{\partial r} \tag{8}$$

where

$$\mu_{rz} = \frac{C'\overline{u'^2}}{C_\varepsilon}\frac{\rho k^{1/2} L}{k}\left[1 - \frac{1}{\overline{u'^2}}\frac{1}{\partial w/\partial r}\frac{g}{T_a}\overline{u'T'}\right] \tag{9}$$

and μ_{rz}/ρ may be identified as the effective or eddy diffusivity for momentum.

In analogy with equation (8), the heat flux term, $\overline{u'T'}$, is written as

$$-\overline{u'T'} = \frac{\mu_T}{\rho}\frac{\partial T}{\partial r} \tag{10}$$

where μ_T/ρ may be visualized as the effective or eddy diffusivity for heat; μ_T is related to μ_{rz} via the relation

$$\sigma_t = \frac{\mu_{rz}}{\mu_T} \tag{11}$$

where σ_t is the turbulent Prandtl number.

Equation (9) contains the normal stress component $\overline{u'^2}$. When the convective and diffusive transport terms are neglected, the exact transport equation for $\overline{u'^2}$ reduces to[7]

$$\overline{u'^2} = Ck \tag{12}$$

where C is a constant. Then, using equations (10) and (12), equation (9) may be written as

$$\mu_{rz} = C_1 \rho (k)^{1/2} L\left[1 + \frac{C_2}{\rho}\frac{\mu_T}{k}\frac{g}{T_a}\frac{\partial T/\partial r}{\partial w/\partial r}\right] \tag{13}$$

where C_1 and C_2 are constants. Also, in analogy with equation (8), the correlation $\overline{u'v'}$ may be written as

$$-\overline{u'v'} = \frac{\mu_{r\theta}}{\rho} r \frac{\partial}{\partial r}\left(\frac{v}{r}\right) \tag{14}$$

where the r–θ viscosity, $\mu_{r\theta}$, is related to μ_{rz} via the r–θ viscosity number given by

$$\sigma_{r\theta} = \frac{\mu_{rz}}{\mu_{r\theta}} \tag{15}$$

The equation for the kinetic energy of turbulence which will be presented later contains the heat flux, $\overline{w'T'}$. When the convective and diffusive transport terms are neglected, the exact transport equation for the correlation $\overline{w'T'}$, using equation (7), reduces to[7]

$$-\overline{w'T'} = \frac{1}{C_\varepsilon C_{1T}}\frac{L}{k^{1/2}}\left[\overline{u'w'}\frac{\partial T}{\partial r} + (1 - C_{2T})\overline{u'T'}\frac{\partial w}{\partial r} - (1 - C_{2T})\frac{g}{T_a}\overline{T'^2}\right] \tag{16}$$

where C_{1T} and C_{2T} are constants.

Equations (13) and (16) require the knowledge of the turbulence kinetic energy, k, the dissipation length scale, L, and the temperature covariance, $\overline{T'^2}$. In this work, the required information has been provided by employing differential transport equations for k, kL and $\overline{T'^2}$. The equations for k and $\overline{T'^2}$ can be derived using the transport equations for the velocity fluctuations u', v' and w' and temperature fluctuation T', respectively. Under the simplifying assumptions already made in deriving equations (1)–(5), the fully modelled equations for k and $\overline{T'^2}$ reduce, respectively, to

$$u\frac{\partial k}{\partial r}+w\frac{\partial k}{\partial z}=\frac{\mu_{r\theta}}{\rho}\left[r\frac{\partial}{\partial r}\left(\frac{v}{r}\right)\right]^2+\frac{\mu_{rz}}{\rho}\left(\frac{\partial w}{\partial r}\right)^2+\frac{g}{T_a}\overline{w'T'}+\frac{1}{\rho r}\frac{\partial}{\partial r}\left(r\frac{\mu_{rz}}{\sigma_k}\frac{\partial k}{\partial r}\right)-C_\varepsilon\frac{k^{3/2}}{L} \tag{17}$$

and

$$u\frac{\partial\overline{T'^2}}{\partial r}+w\frac{\partial\overline{T'^2}}{\partial z}=-2\overline{u'T'}\frac{\partial T}{\partial r}-2C_{3T}\frac{\varepsilon}{k}\overline{T'^2}+\frac{1}{r}\frac{\partial}{\partial r}\left(r\frac{\mu_{rz}}{\sigma_{\overline{T'^2}}}\frac{\partial\overline{T'^2}}{\partial r}\right) \tag{18}$$

in which C_{3T} is a constant σ_k and $\sigma_{\overline{T'^2}}$ may be regarded as the effective Prandtl numbers for k and $\overline{T'^2}$, respectively, and are related to μ_{rz} via the relations

$$\sigma_k=\frac{\mu_{rz}}{\mu_k};\quad \sigma_{\overline{T'^2}}=\frac{\mu_{rz}}{\mu_{\overline{T'^2}}} \tag{19}$$

where μ_k and $\mu_{\overline{T'^2}}$ may be regarded as the effective viscosities for k and $\overline{T'^2}$, respectively.

Following Rodi and Spalding[4] and Lilley,[5] the kL-equation is taken as

$$\mu\frac{\partial kL}{\partial r}+w\frac{\partial kL}{\partial z}=\frac{1}{\rho r}\frac{\partial}{\partial r}\left(r\frac{\mu_{rz}}{\sigma_{kL}}\frac{\partial kL}{\partial r}\right)+\frac{C_B L}{\rho}\left[\mu_{rz}\left(\frac{\partial w}{\partial r}\right)^2\right. \tag{20}$$

$$\left.+\mu_{r\theta}\left\{r\frac{\partial}{\partial r}\left(\frac{v}{r}\right)\right\}^2\right]-C_S k^{3/2}+C_{4T}\frac{gL}{T_a}\overline{w'T'}+C_R\mathrm{Ri}k^{3/2}$$

where C_B, C_S, C_{4T} and C_R are constants, σ_{kL} may be regarded as the effective Prandtl number for kL and

$$\mathrm{Ri}=\frac{\dfrac{2v}{r^2}\dfrac{\partial}{\partial r}(vr)}{\left(\dfrac{\partial w}{\partial r}\right)^2+\left[r\dfrac{\partial}{\partial r}\left(\dfrac{v}{r}\right)\right]^2} \tag{21}$$

may be regarded as the swirling flow Richardson number; σ_{kL} is related to μ_{rz} via the relation

$$\sigma_{kL}=\frac{\mu_{rz}}{\mu_{kL}} \tag{22}$$

where μ_{kL} may be regarded as the effective viscosity for kL.

Equations (8), (10), (13), (14), (16), (17), (18) and (20) may be used to close the set of equations (1)–(5). Since a total of three extra equations have to be solved simultaneously with the equations for mean motion, the turbulence model represents a three-parameter (k–kL–$\overline{T'^2}$) turbulence model.

The numerical values of the 10 model constants and of σ_t, σ_k, σ_{kL}, $\sigma_{r\theta}$ and $\sigma_{\overline{T'^2}}$ appearing in the equations (13)–(22), together with the source from which they are obtained, are presented in Table I. In this table, S_z is the local swirl number to be defined in the next section.

The equation system to be solved is parabolic and, as a result, to determine the solution at any point (r, z), initial orifice conditions ($z = 0, 0 \leqslant r \leqslant r_E$, where E denotes the external boundary) and

Table I. Numerical values of the model constants

Model constants	Value selected	Source
C_1	1·00	Rodi and Spalding[4]
C_B	0·98	
C_S	0·0397	
C_ε	0·055	
σ_k	1·00	
σ_{kL}	1·00	
C_R	0·06	Lilley[5]
$\sigma_{r\theta}$	$1+2S_z^{1/3}$	
C_2	1·95	Chen and Rodi[6]
C_{1T}	3·20	
C_{2T}	0·50	
C_{3T}	0·65	
σ_t	0·70	Chen and Rodi[12]
$\sigma_{T'^2}$	1·00	Taken to be equal to σ_k and σ_{kL}
C_{4T}	0·84	Computer optimization

edge boundary conditions ($z > 0, r = 0$ and $z > 0, r = r_E$) must be given for all the dependent variables. For the inner boundary, I, which for the present case is a symmetry axis, the normal gradients of all the variables are given zero values, the exception being v, which is given a definite zero value. At the outer boundary the specifications for the different variables are

$$u = v = w = p_a - p = T_a - T = k = kL = \overline{T'^2} = 0 \tag{23}$$

on the assumption that the surrounding fluid is stagnant air at uniform temperature and atmospheric pressure.

The initial profiles of w, k, kL, T and $\overline{T'^2}$ have been taken to be uniform (flat) across the section. The initial values of w and T have been chosen to give the desired values of the exit Reynolds and Froude numbers. The initial value of k has given the flow an initial turbulence level of 1 per cent. The initial v-profile has been chosen on the assumption that the fluid is initially in a state of solid body rotation, and the magnitude of the angular velocity has been dependent upon the exit swirl number intended.

THE GOVERNING PARAMETERS

The fluid motion in a jet with swirl and buoyancy is, in general, governed by the inertial, viscous, buoyant and centrifugal forces. The local character of the flow is determined by the relative magnitude of these forces at each point. The overall character of the flow is determined by the strength of the forces at the source and by the ambient conditions.

The ratio of the inertial to viscous forces is called the Reynolds number and, for the conditions at the jet exit, may be written as

$$Re = \frac{w_0 D}{\nu} \tag{24}$$

where D is the diameter of the jet at exit, ν is the kinematic viscosity and the subscript 0 denotes the

exit conditions. The ratio of the buoyant to viscous forces is the Grashoff number, given by

$$G = \frac{g(\rho_a - \rho_0)D^3}{\rho_0 v^2} \tag{25}$$

In a pure jet, only the Reynolds number is of influence, and in a pure plume only the Grashoff number. Turbulent jets and plumes of greatest practical interest are known to have high Reynolds and Grashoff numbers, respectively, so that the viscous forces are negligible in these flows. Therefore, the flow does not depend on these numbers, as long as these are high enough.

No numerical experiments were made for constant values of S (initial swirl number) and F (exit Froude number) with varying values of Re (exit Reynolds number) and G (Grashoff number). However, for all the work reported in the paper, the numerical value of Re was 10,000 or more and that of G at exit was of the order of 10^9 or more.

The ratio of inertial to buoyant forces is called the Froude number (strictly densimetric Froude number) and, for uniform velocity and density profiles at the source, can be defined as

$$F = \frac{w_0^2 \rho_0}{gD(\rho_a - \rho_0)} \tag{26}$$

The Froude number is the most important parameter for turbulent buoyant jets. For pure jet and pure plume, the values of this parameter are infinity and zero, respectively.

Gross transport integrals of the equations (3) and (4) over a cross-section of the jet, after applying the physical boundary conditions cited previously, lead, respectively, to

$$\frac{d}{dz}\int_0^{r_E} \rho v w r^2 dr = -(\rho r^2 uv)_{r=r_E} \tag{27}$$

$$\frac{d}{dz}\int_0^{r_E} \rho\left(w^2 + \frac{p - p_a}{\rho}\right) r dr = g\int_0^{r_E} (\rho_a - \rho) r dr \tag{28}$$

The integrated swirl momentum equation (27) implies that the axial flux of angular momentum in a swirling jet is conserved only when the total circulation at infinity is zero. For a swirling jet emerging into otherwise undisturbed surroundings, a further integration of equation (27) yields

$$\int_0^{r_E} \rho v w r^2 dr = \frac{F_\theta}{2\pi} \tag{29}$$

where F_θ is the constant axial flux of angular momentum.

Equation (28) states that the axial change of flow force, comprised of momentum flux and centrifugal pressure, is due to the effect of buoyancy (i.e. the density difference) only. For a (non-buoyant) swirling jet, the right-hand side of this equation is zero so that

$$\int_0^{r_E} \rho\left(w^2 + \frac{p - p_a}{\rho}\right) r dr = \frac{F_z}{2\pi} \tag{30}$$

where F_z is the constant axial flux of axial momentum, comprised of momentum and pressure terms.

Since both F_θ and F_z are invariants in a (non-buoyant) swirling jet with zero circulation at infinity, they can be used to characterize the jet by defining a strength. A local non-dimensional parameter, called the Local swirl number, may be taken as

$$S_z = \frac{F_\theta}{F_z r_E} \tag{31}$$

where r_E is the local external radius of the jet. It has an initial orifice value of

$$S = \frac{F_\theta}{F_z D/2} \tag{32}$$

where D is the exit diameter of the jet. In a swirling jet S_z decreases progressively in the downstream direction, the asymptotic case being that of a non-swirling flow, and at any axial location it characterizes the effect of rotation on the flow.

The swirling jets have often been classified based on the magnitude of the initial swirl parameter. As S is increased from its non-swirling value (= 0) to higher values, the cases of weak, moderate and strong swirling jets are presented. For weak swirl ($0 < S \leqslant 0{\cdot}20$), the pressure variations are small (and even negligible), the coupling between the equations is small and the simplified boundary layer equations considered in this work are valid. For moderate swirl ($0{\cdot}20 < S \leqslant 0{\cdot}50$), the simplified boundary layer equations including pressure variations are somewhat questionable, but are still used,[12] for present-day knowledge of turbulence necessitates similar approximations elsewhere in any analysis. A strong swirling jet ($S > 0{\cdot}5$) possesses strong radial and axial pressure gradients in the regions near the orifice and the axial one is sufficient to cause a recirculation zone to be set up in the region of the orifice.[14] Evidently the reduced boundary layer equations will not be valid here and the full equations must be solved.[15]

THE PREDICTION PROCEDURE

The reduced boundary layer equations (1)–(5), (17), (18) and (20) are parabolic and highly coupled. Recently, powerful numerical techniques have been evolved for solving such systems of equations accurately and economically. One of them is the fully-implicit finite difference forward-marching prediction procedure embodied in GENMIX.[16] GENMIX is a general computer program for predicting steady two-dimensional boundary layer flows and the embodied numerical technique is stable, accurate and economical. A non-dimensional stream function is employed as the independent variable across the layer and the main novelty lies in the choice of grid, which adjusts its width automatically at each forward step so as to conform to the thickness of the layer in which significant variations are present. Consequently, the numerical prediction procedure embodied in GENMIX has been used to solve the reduced boundary layer equations considered in this work. Here only the highlights of the numerical scheme used are considered. Modifications of the basic procedure to solve the swirl momentum equation satisfactorily can be found in Reference 11 and the details of the basic scheme, together with program listings, can be found in References 13 and 16.

Since the solution procedure embodied in GENMIX employs the non-dimensional stream function as the cross-stream independent variable, the governing equations are first transformed from (r, z) co-ordinates to von Mises (ψ, z) co-ordinates. In the von Mises co-ordinate system the governing equations possess the common form

$$\frac{\partial \phi}{\partial z} = \frac{\partial}{\partial \psi}\left(\rho r^2 w \mu_\phi \frac{\partial \phi}{\partial \psi}\right) + \frac{1}{\rho w} S_\phi \tag{33}$$

where ϕ stands for any of the dependent variables w, T, k, kL and $\overline{T'^2}$, μ_ϕ is the effective viscosity for ϕ and S_ϕ represents the source term in the ϕ-equation. Rather than expressing the swirl momentum equation (3) in this form, the diffusion term of that equation may be rewritten in terms of v/r so as to eliminate the large source term which is a cause of great inaccuracy in any numerical solution

procedure. The swirl momentum equation then becomes

$$\frac{\partial vr}{\partial z} = \frac{\partial}{\partial \psi}\left[\rho r^4 w \mu_{r\theta} \frac{\partial}{\partial r}\left(\frac{v}{r}\right)\right] \tag{34}$$

In the Patankar–Spalding numerical scheme, equations (33) and (34) are further transformed from von Mises (ψ, z) co-ordinates to (ω, z) co-ordinates where

$$\omega = \frac{\psi - \psi_I}{\psi_E - \psi_I} \tag{35}$$

is the non-dimensional stream function the value of which always lies between 0 (at the inner edge, I) and 1 (at the outer boundary, E).

The variation of ω from the inner to the outer boundary is assumed to be linear. To ensure that the conservation condition is satisfied, each differential equation is integrated over a small control volume extended half-way between the adjacent grid points. On the assumption that any dependent variable ϕ varies linearly with ω between grid points and making use of the unknown downstream ϕ-values (so as to use a fully-implicit scheme), the general ϕ-equation (33) and the swirl momentum equation (34) yields the general finite difference equation

$$D_i \phi_{i,D} = A_i \phi_{i+1,D} + B_i \phi_{i-1,D} + C_i \tag{36}$$

in which the coefficients A_i, B_i, C_i and D_i at the ith grid point, which are different for different equations, can be evaluated from the quantities which are known at the upstream station. By substituting

$$P_2 = A_2/D_2$$

$$Q_2 = \frac{B_2\phi_1 + C_2}{D_2}$$

$$P_i = \frac{A_i}{D_i - B_i P_{i-1}}, \quad i = 3, 4, \ldots, N-1$$

and

$$Q_i = \frac{B_i Q_{i-1} + C_i}{D_i - B_i P_{i-1}}, \quad i = 3, 4, \ldots, N-1 \tag{37}$$

where N is the total number of cross-stream grid points including the boundary values, it is easy to show that equation (36) satisfies the equation

$$\phi_i = P_i \phi_{i-1} + Q_i \tag{38}$$

For each step in Δz downstream, the coefficients P_i and Q_i can be evaluated from known upstream values, beginning with the initial orifice values, and, since the grid edge values of the dependent variables are known, equation (38) can be solved for all the values of the dependent variables in turn at each successive downstream grid location. In this way, the solution can be marched downstream as far as required.

The incorporation of swirl can cause significant variation of pressure in the axial direction, particularly when the swirl is strong and an accurate solution of the axial momentum equation (4) demands that the pressure at each downstream grid location be evaluated as accurately as possible. As a result, the swirl momentum equation (3) was solved first so that the downstream pressure gradient could be evaluated accurately. The axial momentum equation and the equations for k, kL, T and $\overline{T'^2}$ were then solved in turn.

The computer time for solving six equations up to 220 downstream steps for $N = 40$ and $\Delta z = 0{\cdot}1 r_E$ on the CDC 7600 computer was about four seconds. This represents a speed of about 330 equations per step per second.

RESULTS AND DISCUSSION

The proposed turbulence model has been shown to be capable of reproducing, with the same values of the model constants, the gross features of pure jet flows, buoyant flows and swirling flows for weak and moderate swirl. For strong swirl, however, the predicted results have indicated a progressive decline, with increased swirl, in the ability of the model to describe the experimental data accurately. Thus, the simplified boundary layer equations of the second section, based on the assumption that $\partial/\partial r \gg \partial/\partial z$, do not seem to be valid for a strong swirling jet and the full equations have to be solved.

The results predicted by the proposed turbulence model and presented in Figures 1–7 indicate that, at any downstream location, the behaviour of a turbulent swirling jet in uniform and stagnant surroundings and under the action of buoyancy forces, is determined solely by two physical parameters associated with the source conditions—the initial swirl number, S, and the exit Froude number, F. When the initial swirl number is low ($S \leqslant 0{\cdot}2$) and exit Froude number is high ($F \geqslant 100$), the jet spreads linearly in the axial direction and the profiles of the mean quantities exhibit similarity behaviour in an initial region relatively close to the jet exit. The flow characteristics of this similarity region are more or less the same as those in the corresponding region of a (non-buoyant) swirling jet. This is because for high exit Froude numbers the effect of buoyancy is felt at some considerable distance downstream of the jet exit and the flow characteristics in the initial region are affected very little by buoyancy. For high initial swirl numbers and or low exit Froude numbers the predicted results indicate that a true similarity of the flow in the initial region is not possible.

In the far field where the magnitude of the swirl velocity becomes negligibly small, the jet turns to a buoyancy-dominated plume in which the profiles of the mean and turbulent quantities exhibit true similarity behaviour and the jet spreads linearly in the axial direction. The flow characteristics of this far-field similarity region correspond closely to those in the plume region of a buoyant jet and are not affected by the initial conditions. Thus, the asymptotic case of a swirling jet in uniform and stagnant surroundings and under the action of buoyancy forces is a pure plume in the far field, a fact first reported by Lee.[1]

The axial development of the velocity half-width, $r_{0.5w}$, defined as the value of r at which the axial velocity reduces to one-half of its maximum value, is presented in Figure 1. For a given degree of swirl, a low exit Froude number causes the jet to grow in its width at a considerably high rate in the initial region of the jet. The axial location at which the jet starts to grow in its width seems to be the beginning of the intermediate region (the region of transition between the initial non-buoyant and final buoyant regions) of the jet at which the buoyancy forces start to operate on the flow. The available experimental data suggest that the location of the start of the intermediate region of a (non-swirling) buoyant jet is given by[12]

$$\frac{z + z_0}{D} = 0{\cdot}5 F^{1/2} (\rho_0/\rho_a)^{1/4} \tag{39}$$

where z_0 is the axial distance of the virtual origin from the jet exit. This location of the beginning of the intermediate region of a buoyant jet seems to hold for a buoyant swirling jet also. From Figure 1 it is readily seen that, in the first ten exit diameters or so of the intermediate region, the rate of spread of the velocity half-width (and hence of the jet width) is considerably higher than that in

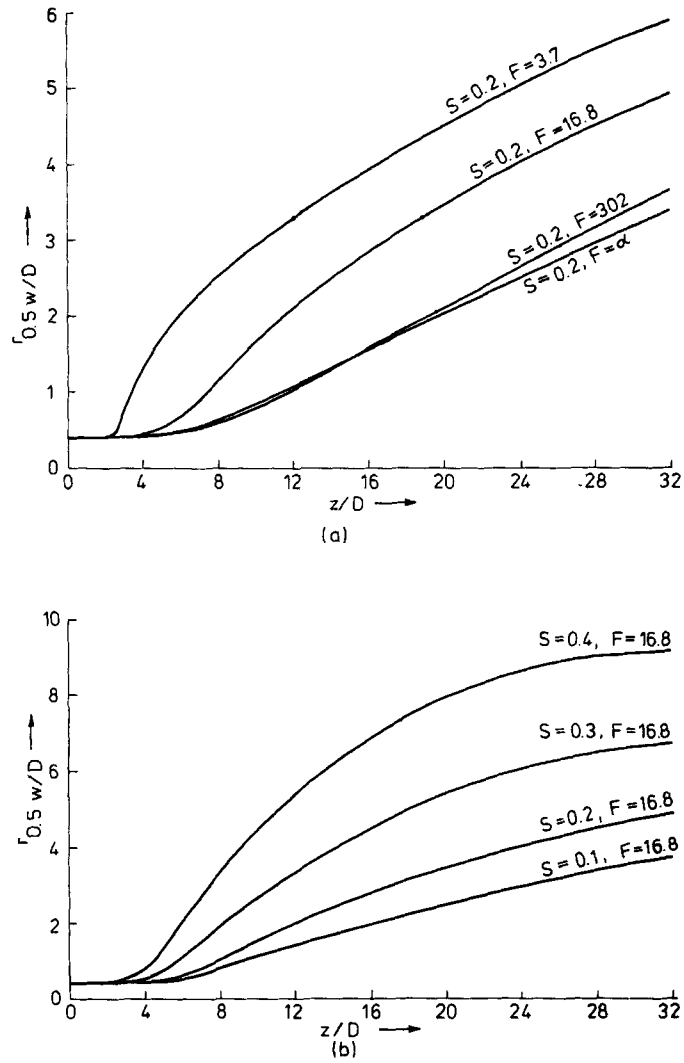

Figure 1. Axial development of the velocity half width for various values of exit swirl and Froude numbers

the corresponding region of a (non-buoyant) swirling jet. It will be shown later in this section that at the onset of the intermediate region the jet entrains the ambient fluid, due to the introduction of buoyancy forces, at a rate which is considerably higher than that in a non-buoyant jet. Owing to this rapid increase in the mass flow rate and the presence of swirl, a rapid mixing of the entrained fluid with the jet fluid takes place and this rapid mixing is characterized by the higher rates of growth of the velocity and temperature half-widths and a higher rate of decay of the swirl velocity. Introduction of buoyancy in Narain and Uberoi's[2] integral model also results in exceptionally large mixing which acts to produce a large rate of spread, consequently increasing the decay of the azimuthal velocity.

From Figure 1 it is seen that, after about ten exit diameters of the intermediate region, the flow in the low Froude number jet seems to be more or less established and the rate of spread of the velocity half-width remains more or less constant for some distance downstream. This region of

established flow possibly corresponds to that region in a swirling jet in which the swirling flow shows similarity behaviour but the rate of spread, $\delta_w (= dr_{0.5w}/dz)$ in the former is higher than that in the latter because the effect of buoyancy is to increase the rate of spread δ_w in a buoyant jet over that in a non-buoyant jet. After this flow-established region, the rate of spread δ_w decreases gradually with downstream distance due to the weakening of swirl and finally reduces to the constant plume-similarity value ($= 0{\cdot}110$) in the far field.

For high exit Froude numbers the flow exhibits similarity behaviour in the initial region of the jet in which the flow parameters behave as in the corresponding similarity region of a (non-buoyant) swirling jet. This is because when the exit Froude number is high, the intermediate region starts some distance downstream, the location being determined by using equation (39), and the flow characteristics in the initial region are not affected by buoyancy. At the start of the intermediate region, the mass flow rate does not increase appreciably because of the weak buoyancy strength of the

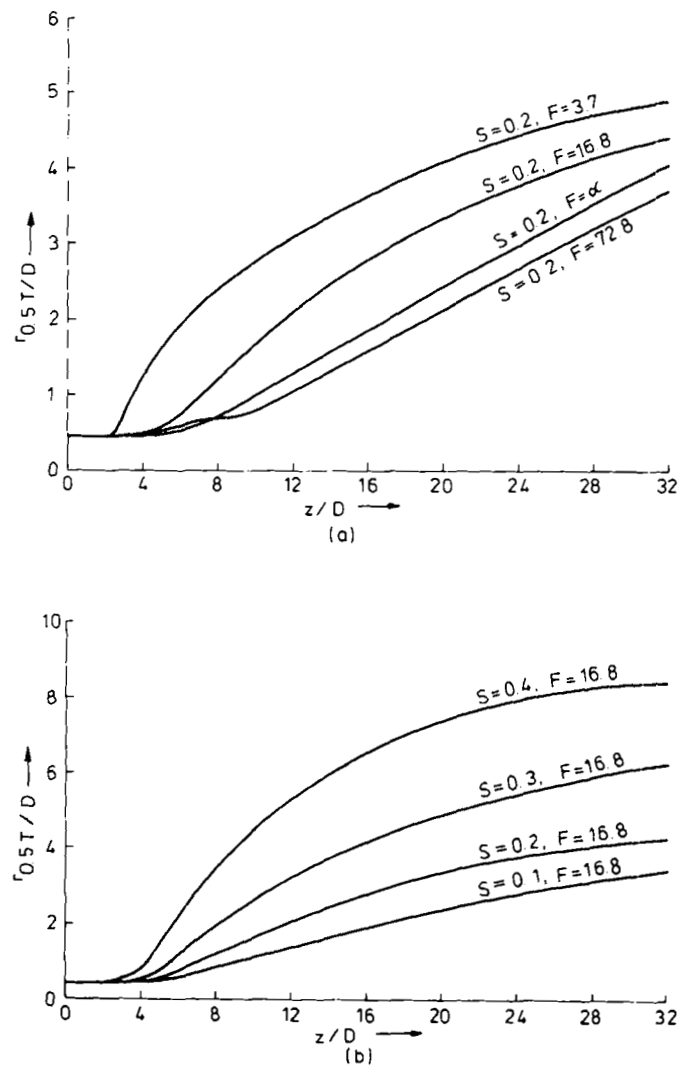

Figure 2. Axial development of the temperature half width for various values of the exit swirl and Froude numbers

jet. Since the swirl velocity decays as being proportional to z^{-2} in the initial non-buoyant region,[14] the magnitude of this velocity at the onset of the intermediate region is also small compared to its initial value. As a result, the incorporation of buoyancy in a high Froude number swirling jet does not produce any significant change in the rate of spread of the velocity half-width of the jet, rather the velocity half-width increases gradually for a distance downstream due to the action of buoyancy. Further downstream the axial growth of the velocity half-width is the same as that in a low Froude number jet.

From Figure 1 it is readily seen that, for a given exit Froude number, a higher rate of spread, δ_w, is always associated with a higher exit swirl number in the initial region of the jet, a result which was also predicted by Lee,[1] Narain and Uberoi[2] and Ross.[3] In the final plume similarity region, however, δ_w approaches a constant value ($=0{\cdot}110$) irrespective of the initial degree of swirl.

The axial variation of the temperature half-width, $r_{0.5T}$, defined as the value of r at which the temperature excess $(T-T_a)$ reduces to one-half of its maximum value, for various values of the exit Froude and swirl numbers are shown in Figure 2. The temperature half-width shows the similar variation in the axial direction to that of the velocity half-width with the exit Froude and swirl numbers except that the incorporation of buoyancy causes the rate of spread $\delta_T (= \mathrm{d}r_{0.5T}/\mathrm{d}z)$ to decrease in a buoyant jet than that in a non-buoyant jet, although for the rate of spread δ_w the reverse is true.

Lee[17] reported the experimentally determined values for the constant rates of spread δ_w and δ_T in the initial similarity region of a buoyant swirling jet for the case when $S \simeq 0{\cdot}1$ and $F \simeq 250$. For these values of the two source parameters, the proposed model predicts $\delta_w = 0{\cdot}097$ and $\delta_T = 0{\cdot}112$ which are in good agreement with the corresponding values of 0·100 and 0·116 reported by Lee.[17] The profiles of the mean axial velocity, swirl velocity and temperature predicted by the present model for the case when $S = 0{\cdot}1$ and $F = 302$ have been plotted in Figure 3 (the subscript 'm' denoting the maximum value) and compared with the experimental data of Lee[17] for $S \simeq 0{\cdot}1$ and $F \simeq 250$. The agreement between the predicted profiles and the experimental data is satisfactory.

The axial decay of the centreline (or maximum) axial velocity for various values of the exit Froude and swirl numbers is shown in Figure 4. For low exit Froude numbers the centreline velocity increases with downstream distance in the initial core-flow region, a fact predicted by Lee[1] and Chen and Nikitopoulos.[10] After this core-flow region, the axial velocity starts to decay and initially the rate of decay is very high compared to that in any other region of the jet. A comparison of Figure 4 with Figure 1 shows that this high rate of decay of the axial velocity (and the associated high rates of spread) occurs at the beginning of the intermediate region as a result of the large mixing of the entrained fluid with the jet fluid. Further downstream the rate of decay of the axial velocity is gradually reduced by the action of buoyancy until it decays finally as $z^{-1/3}$ in the plume-similarity region. For high exit Froude number, after an initial core flow region, the axial velocity starts to decay as z^{-1} as in a non-buoyant jet. However, in the intermediate region the decay rate is gradually reduced by the buoyancy force until in the plume-similarity region it decays as $z^{-1/3}$. The high rate of decay of the axial velocity in a low Froude number jet at the beginning of the intermediate region is in qualitative agreement with the results predicted by Lee[1] and Narain and Uberoi,[2] whereas, in a high Froude number jet, the introduction of buoyancy reduces the rate of decay of the axial velocity, a result predicted both by Lee[1] and Ross.[3] Unfortunately the above results could not be compared with Lee's[17] data because his initial conditions cause the axial velocity to decay immediately after the jet exit showing no potential core flow.

From Figure 4 it is seen that a higher initial swirl causes the decay of the axial velocity more rapidly in the initial region. The rate of decay gradually reduces with downstream distance for all degrees of swirl although the rate of decrease is higher for a higher initial swirl. As a result the rate of decay of the axial velocity becomes slower with a higher degree of swirl further downstream until,

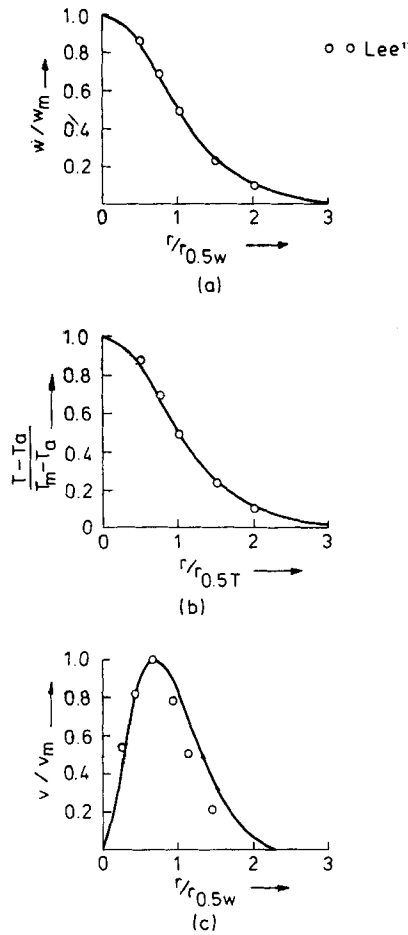

Figure 3. Profiles of the axial velocity, temperature and swirl velocity at z/D = 10 for F = 302 and S = 0·1

in the plume-similarity region, the axial velocity decays as $z^{-1/3}$ for all degrees of swirl. The above results are in qualitative agreement with those predicted by Lee,[1] Narain and Uberoi[2] and Ross.[3]

The axial decay of the centreline (or maximum) temperature for different values of the exit Froude and swirl numbers is presented in Figure 5. Unlike the axial velocity, the maximum temperature never increases from its exit value in the initial core-flow region, a result predicted by Chen and Nikitopoulos[10] for buoyant jets. For low exit Froude number, the decay of temperature starts closer to the jet exit and, for the reasons already stated, the rate of decay is relatively high at the beginning of the intermediate region. With an increase in the downstream distance, the rate of decay is gradually reduced until, in the final region, the temperature decays as $z^{-5/3}$. For high exit Froude numbers, the axial decay of temperature is delayed in the initial region but once the decay starts, it takes place at a rather steep slope. Further downstream the rate of decay is the same as in the low Froude number case. The above findings for the decay of the maximum temperature are in qualitative agreement with the predictions of Lee.[1]

From Figure 5 it is seen that, in the initial region, a higher rate of decay of the maximum temperature is always associated with a higher degree of swirl. Further downstream, however, the

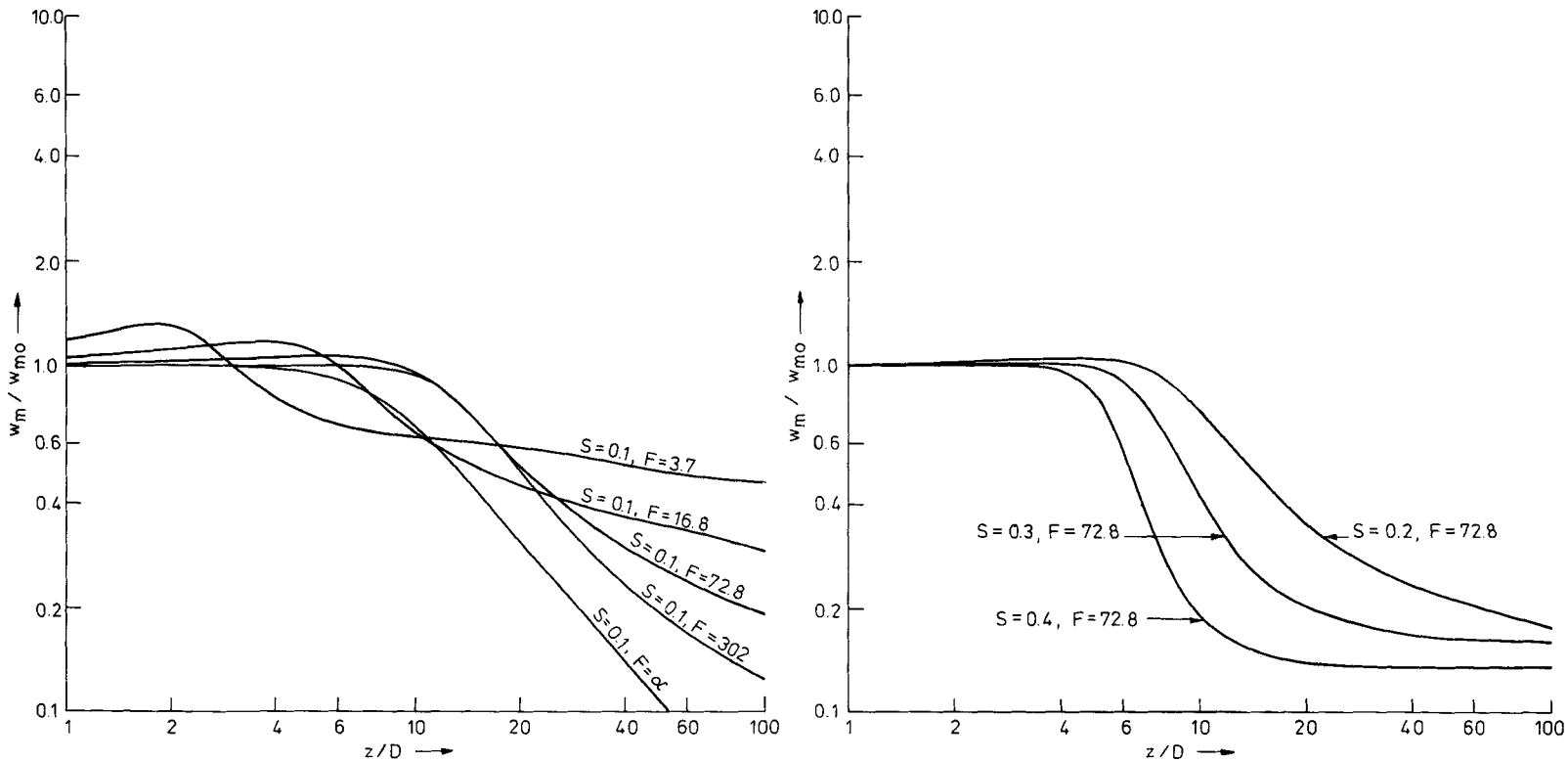

Figure 4. Axial decay of the centreline axial velocity for various values of the exit swirl and Froude numbers

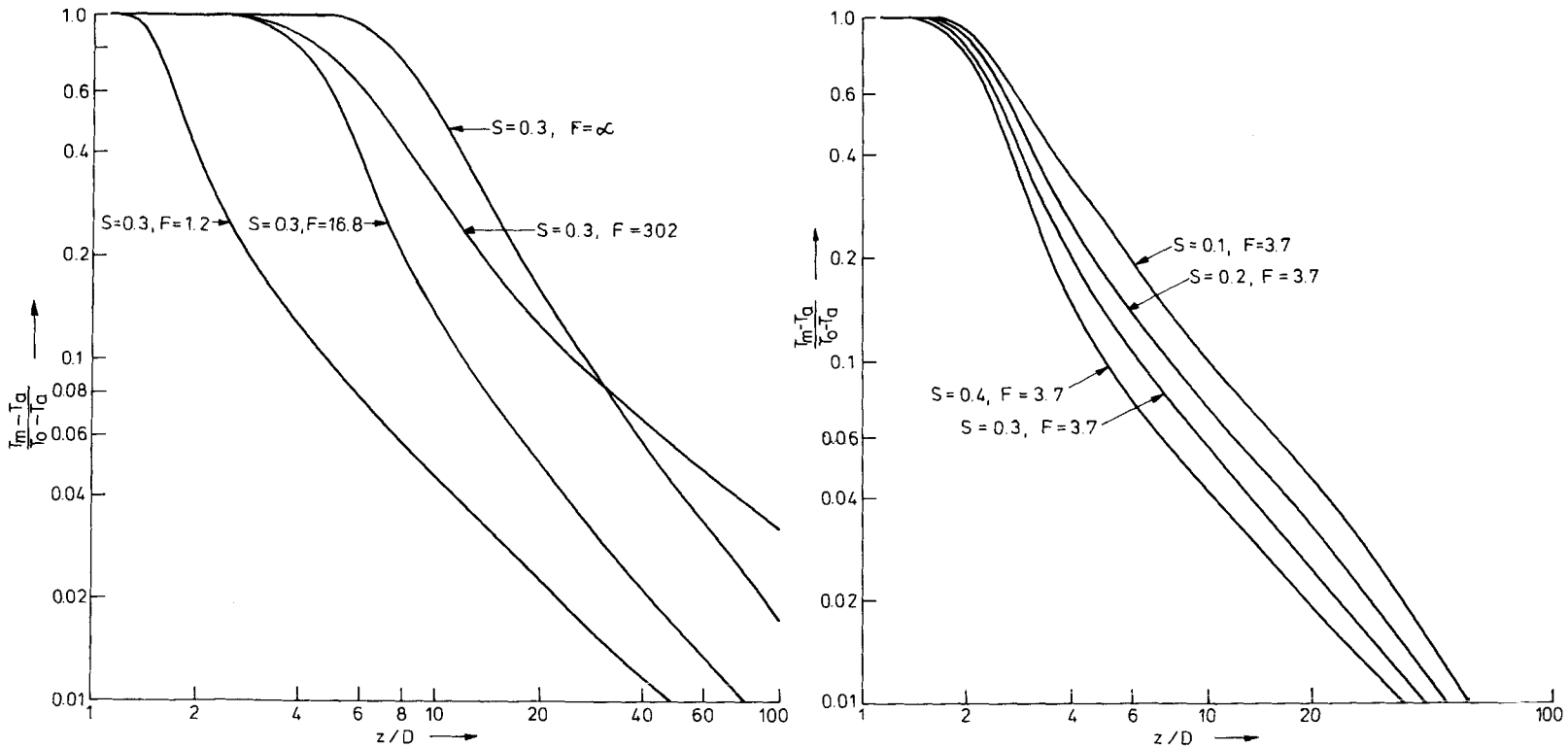

Figure 5. Axial decay of the maximum temperature for various values of the exit swirl and Froude numbers

rate of decay rather decreases with a high degree of swirl. These predictions are also in qualitative agreement with those of Lee.[1]

The axial developments of the maximum swirl velocity for various values of the exit Froude and swirl numbers are shown in Figure 6. For a high exit Froude number, the decay of swirl velocity is reduced by the action of buoyancy, a fact that is in qualitative agreement with the predictions of Lee[1] and Ross.[3] For the case when $S = 0{\cdot}1$ and $F = 302$, the predicted results are found to be in good agreement with the experimental data of Lee[17] for $S \simeq 0{\cdot}1$ and $F \simeq 250$. For low exit Froude numbers the maximum swirl velocity remains constant or increases from its exit value in a short region close to the jet exit. This peculiar decay characteristic of the swirl velocity for low exit Froude numbers was first predicted by Lee[1] and is similar to that of the axial velocity shown in Figure 4. After this short core region, the swirl velocity decays very rapidly. As stated earlier, this rapid decay of the swirl velocity is a result of the large mixing of the entrained and jet fluids at the start of the intermediate region and is in qualitative agreement with the results predicted by Narain

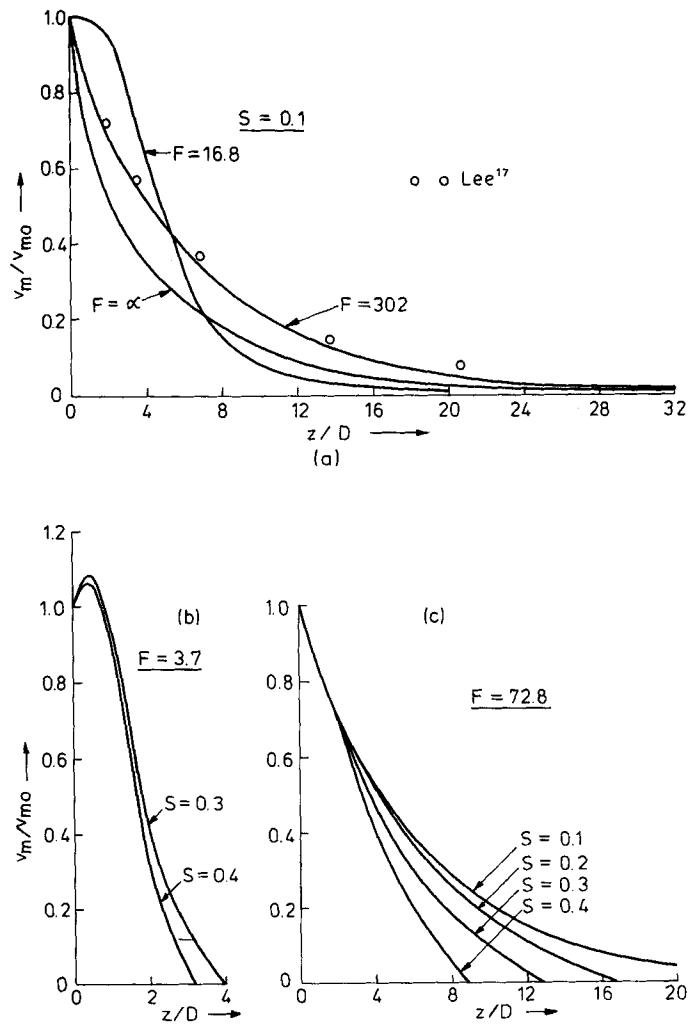

Figure 6. Axial decay of the maximum swirl velocity for various values of the exit swirl and Froude numbers

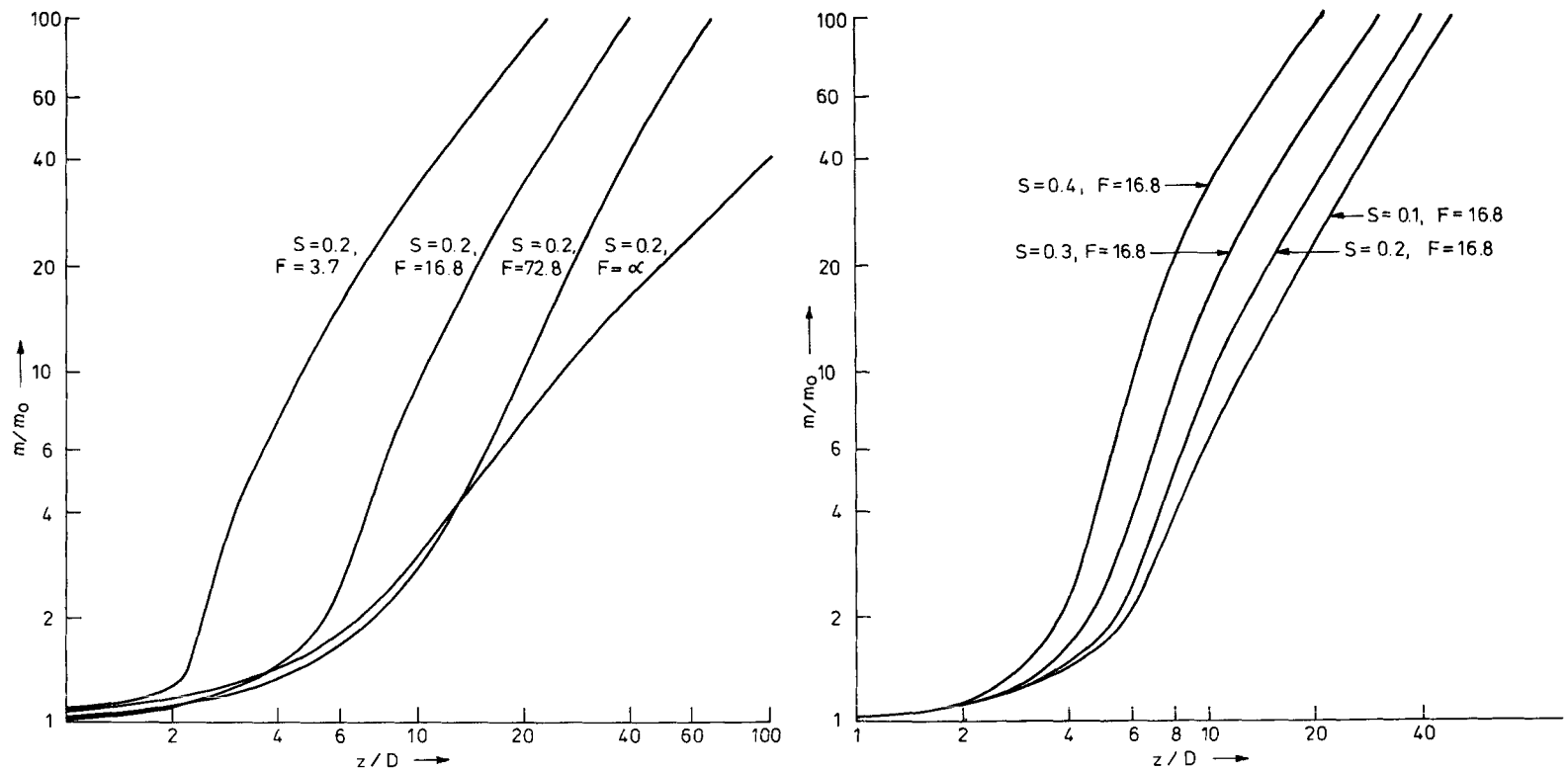

Figure 7. Axial variation of the mass flow rate for various values of the exit swirl and Froude numbers

and Uberoi.[2] From Figure 6 it is also observed that, for a given exit Froude number, the decay of the swirl velocity is quicker for a higher initial swirl and vice versa and this is in qualitative agreement with the results predicted by Lee,[1] Narain and Uberoi[2] and Ross.[3]

The axial variation of the mass flow rate for various values of the exit Froude and swirl numbers is shown in Figure 7. For a given exit swirl number, the mass flow rate of the jet increases with an increase in the buoyancy strength (i.e. with a decrease in the value of F) and for low exit Froude numbers the mass flow rate is considerably higher, particularly in the initial region, than that in a non-buoyant jet. A comparison of Figure 7 with Figure 1 indicates that this rapid increase in the mass flow rate begins to occur at the start of the intermediate region due to the action of buoyancy and in the first ten exit diameters or so of the intermediate region, the mass flow rate is considerably higher than that in any other region of the jet. Both the Narain and Uberoi[2] and Ross[3] models predicted mass flow rates which are higher than those in a corresponding (non-bouyant) swirling jet, although the mass flow rates predicted by Narain and Uberoi are considerably higher than those predicted by Ross.

From Figure 7 it is readily seen that, for a given exit Froude number, the mass flow rate is higher for a higher initial degree of swirl, a result predicted both by Narain and Uberoi[2] and Ross[3] models.

CONCLUDING REMARKS

The aim of the present work has been to develop a three-parameter (k–kL–$\overline{T'^2}$) model of turbulence applicable to free boundary layers and use it for the predictions of the flow characteristics of a swirling jet in uniform and stagnant surroundings under the action of buoyancy forces. The model is capable of reproducing many features of pure jet flows, buoyant flows and swirling flows for weak and moderate swirl. For strong swirl the simplified boundary layer equations do not seem to be valid as indicated by a progressive decline in the ability of the turbulence model to describe the experimental data accurately.

The results of the numerical investigation presented in Figures 1–7 indicate that the incorporation of buoyancy can produce significant changes in the behaviour of a turbulent swirling jet in uniform and stagnant surroundings, particularly for high buoyancy strengths, affecting the growth of the jet width, the axial decay of the mean quantities, the mass flow rates and so on. The behaviour of the jet at any downstream location depends solely on the exit swirl and Froude numbers. The predicted results have been found to be in satisfactory agreement with available experimental data and in qualitative agreement with other theoretical results and may help, at the end, to control the flow under investigation.

During the course of the present work it has become quite apparent that the state of experimental knowledge is much less satisfactory for jets with swirl and buoyancy effects than for pure, swirling and buoyant jets. The validity of a turbulence model can be tested only when sufficient reliable and accurate experimental data are available. The results presented in Figures 1–7 have indicated that incorporation of buoyancy has a considerable effect on the flow characteristics of a swirling jet and sufficient and reliable experimental data are necessary to make a final judgement.

ACKNOWLEDGEMENTS

One of us (M.A.H.) gratefully acknowledges the financial support given by the Commonwealth Scholarship Commission in the United Kingdom during the course of this work.

REFERENCES

1. S. L. Lee, 'Axisymmetrical turbulent swirling natural convection plume. Part I—theoretical investigation', *Trans. A.S.M.E., J. Appl. Mech*, **33,** 647–655 (1966).
2. J. P. Narain and M. S. Uberoi, 'The swirling turbulent plume', *Trans. A.S.M.E., J. Appl. Mech.*, **41,** 337–342 (1974).
3. D. G. Ross, 'On integral-method solutions for modelling swirling jets and plumes', *Appl. Sci. Res.*, **34,** 273–298 (1978).
4. W. Rodi and D. B. Spalding, 'A two-parameter model of turbulence, and its application to free jets', *Warme-und-Stoffubertragung*, **3,** 85–95 (1970).
5. D. G. Lilley, 'Prediction of inert turbulent swirl flows', *AIAA J.*, **11,** 955–960 (1973).
6. C. J. Chen and W. Rodi, 'A mathematical model for stratified turbulent flows and its application to buoyant jets', *16th IAHR Congress*, Sao Paulo, Brazil, 1975.
7. B. E. Launder, 'On the effects of a gravitational field on the turbulent transport of heat and momentum', *J. Fluid Mech.*, **67,** 569–581 (1975).
8. I. K. Madni and R. H. Pletcher, 'Prediction of turbulent forced plumes issuing vertically into stratified or uniform ambients', *Trans. A.S.M.E., J. Heat Transfer*, **99,** 99–104 (1977).
9. B. E. Launder and A. Morse, 'Numerical prediction of axisymmetric free shear flows with a Reynolds stress closure', *1st Symp. on Turbulent Shear Flow*, Springer-Verlag, Berlin, 1979, pp. 279–294.
10. C. J. Chen and C. P. Nikitopoulos, 'On the near field characteristics of axisymmetric turbulent buoyant jets', *Int. J. Heat Mass Transfer*, **22,** 245–255 (1979).
11. M. A. Halim, 'Turbulent mass, momentum and heat transfer in atmospheric boundary layers', *Ph.D. Thesis*, University of Manchester, 1982.
12. C. J. Chen and W. Rodi, *Vertical Turbulent Buoyant Jets—a Review of Experimental Data*, Pergamon Press, Oxford, 1980.
13. S. V. Patankar and D. B. Spalding, *Heat and Mass Transfer in Boundary Layers*, 2nd Edn, Intertext, London, 1970.
14. N. A. Chigier and A. Chervinsky, 'Experimental investigation of swirling vortex motion in jets', *Trans. A.S.M.E., J. Appl. Mech.*, **34,** 443–451 (1967).
15. A. D. Gosman, W. M. Pun, A. K. Runchal, D. B. Spalding and M. Wolfshtein, *Heat and Mass Transfer in Recirculating Flows*, Academic Press, London, 1969.
16. D. B. Spalding, *GENMIX—a General Computer Program for Two-dimensional Parabolic Phenomena*, Vol. 1, Pergamon Press, Oxford, 1977.
17. S. L. Lee, 'Axisymmetrical turbulent swirling natural convection plume. Part 2—experimental investigation', *Trans. A.S.M.E., J. Appl. Mech.*, **33,** 656–661 (1966).